A Revisit to Model-Free Control

Wanrong Li, Huawei Yuan, *Member, IEEE*, Sinan Li, *Member, IEEE*, and Jianguo Zhu, *Senior Member, IEEE*

***Abstract*—Starting from Fliess's model-free control (MFC) technique developed 15 years ago, this article aims to provide a systematic framework for characterizing, benchmarking, and generalizing this emerging control technique, with a particular focus on power electronics (PE). It examines the performance of MFC in terms of dynamic response, stability, and robustness, using the classical control theory as a basic tool. A theoretical comparison is conducted with the conventional linear control techniques on dynamic response and performance robustness. A generalized MFC theory and means to enhance its robustness performance are also highlighted. This article suggests that MFC, in contrast to the conventional understanding based on model-independent error dynamics, is practically a model-based control technique. Such model dependence characteristics under MFC become more severe for PE systems. However, following a new design principle, MFC is found possible to possess extraordinarily robust performance against model variations as compared to most existing model-based control methods. On top of that, stability margin is found to be the key bottleneck hindering the performance robustness of the existing MFC techniques. A new MFC with greater stability margin and performance robustness is proposed in this article. Comprehensive Pareto fronts analysis, simulations, and experiments are conducted on a buck converter system to verify the new understandings and conclusions drawn from the framework. With the new design principle and the new MFC, the system is able to demonstrate an almost constant dynamic response despite 25-fold circuit parameter (*R, C*, and *L*) variations and 1.85-fold input voltage variations.**

***Index Terms*—Buck converter, model uncertainty, model-free control, pareto fronts, performance robustness, power electronics controller design automation, sensitivity.**

I. Introduction

AUTOMATIC control based on the principles of feedback was first introduced to an industrial process by James Watt for speed control of a steam engine over two centuries ago. Since then, controllers have become ubiquitous in almost every industry, including power electronics (PE), chemical, automobile, and steel industries, among others. Despite its long history of evolvement, the ultimate goal of control systems has been the same: realizing optimal system performance (typically in terms of stability, steady-state and dynamic performance, and robustness) while being cost-effective and simple to design [1].

Traditionally, control methods can be classified as linear and nonlinear [2]. At present, linear control techniques, e.g., the proportional-integral-derivative (PID) controller, dominate many practical industrial (including PE) systems, mainly due to their lower implementation cost, fewer tuning parameters, and longer history of utilization than nonlinear controllers [3]–[5]. On the other hand, nonlinear control techniques (e.g., adaptive control [6]), robust control (e.g., sliding mode control) [7], and optimal control (e.g., model-predictive control) [8], etc., are also of great importance in the control of industrial processes, mainly because they can improve the system robustness against work environment changes, and/or system parameter variations, and/or constraints demanded in the manufacturing process, as compared to linear controllers [9], [10]. However, the above-mentioned control methods are all model-based, meaning that their success highly relies on: i) the accuracy of the nominal or initial guess of the mathematical model of the controlled plant, and/or ii) the assumptions about the model uncertainties, e.g., *a priori* bounds, distributions, and/or configurations of uncertainties (usually additive and multiplicative descriptions). As a result, today's design process of these traditional controllers in practice still involves significant iterations of modeling, tuning, and testing that often demand enormous time, expertise, and resources, resulting in long and costly design cycles [11]. Such a design process is not conducive to the low-cost, fast-paced development cycles required for today's technology deployment [12]. For instance, in the fields of PE, the "speed" bottleneck of controller design has been severe enough to lead to the organization of two IEEE special workshops in the *IEEE Energy Conversion Congress and Exposition* to address this controller design challenge in 2018 and 2019. Particularly, in the 2019 workshop, controller design and testing were explicitly identified as the most important step to be automated in the current PE design process [13].

A new trend of model-free control (MFC) has been gathering momentum in the past three decades. The ultimate aim of MFC is to reduce the number of design cycles and the cost of the controller design process by achieving: 1) *model-free design* such that the dynamics and stability performance of a system can be precisely controlled through the design of the controller only, requiring no knowledge of the plant model, and 2) *model-free operation* such that the dynamics and stability performance of a system is robust against plant model variations. On the one hand, these capabilities of MFC may help increase the occurrences of first-pass design success without the need for iterative and manual testing, ideally allowing for a fully automated design

Manuscript received 18 April 2022; revised 3 July 2022; accepted 4 August 2022. Date of publication 9 August 2022; date of current version 6 September 2022. This work was supported by the Australian Research Council under Grant DP220100231. Recommended for publication by Associate Editor C. Tse. *(Corresponding author: Sinan Li.)*

Wanrong Li, Sinan Li, and Jianguo Zhu are with the School of Electrical and Information Engineering, University of Sydney, Camperdown, NSW 2006, Australia (e-mail: wanrong.li@sydney.edu.au; sinan.li@sydney.edu.au; jianguo.zhu@sydney.edu.au).

Huawei Yuan is with the School of Electrical and Information Engineering, Nanyang Technological University, Singapore 639798 (e-mail: hwyuan@connect.hku.hk).

Color versions of one or more figures in this article are available at https://doi.org/10.1109/TPEL.2022.3197692.

Digital Object Identifier 10.1109/TPEL.2022.3197692

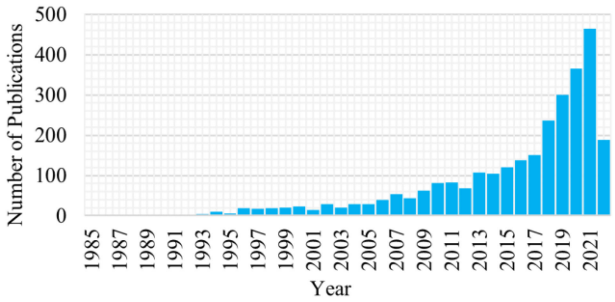

Fig. 1. Number of annual publications related to MFC since 1985 for electrical and electronics. The statistical data are based on searching the IEEE Xplore, and the data for 2022 are up to June 2022. As a result, a total of 2849 relevant conference and journal papers were identified.

process of PE controllers. On the other hand, such capabilities suggest the possibility to realize plug-and-play control—the same controller can be directly used across different product lines with drastically different circuit parameters without the need for a completely new controller development cycle.

Fig. 1 shows the number of annual publications related to MFC in electrical and electronics engineering (EEE) since 1985. As shown, the research on MFC has increased dramatically, especially in recent years. Notably, MFC was originated outside the field of EEE but is now widely applied to the control of various devices and systems, such as smart grids [14], permanent magnet synchronous motors [15], robotic systems [16], vehicular systems [17], and PE [18], [19], [20], [21], [22], [23], [24].

This article revisits an MFC technique based on the concept of the local-affine model (or ultralocal model in the literature), proposed by Fliess et al. [25], [26], with a specific focus on its implications for future PE controller design automation research. Although other MFC methods exist in the literature, such as artificial intelligence control [27] and model-free adaptive control [28], etc., we focus on this particular MFC method due to its simple structure and low computational cost, which are of great importance to fast-dynamics and cost-sensitive applications. Research into such a type of MFC for PE systems is still at its early stage. MFC is implemented in dc–dc converters for the first time in [18], in which MFC is reported to have improved stability and disturbance rejection capability against load and input voltage variations. In recent years, MFC has been employed in a wider range of PE applications such as PFC [19], HVDC [20], battery energy storage [21], and PV systems [22], etc. It is reported that MFC can improve PF and lower the THD while achieving faster tracking performance and smaller overshoot during transients, such as a startup, parameter variations, and fault recovery, compared with traditional model-based controllers. In [23] and [24], MFC is further combined with model predictive control (MPC) to obtain fast and robust dynamics in power converter applications. These studies show that applying MFC to PE applications can achieve superior performance in terms of reference tracking bandwidth and disturbance rejection capability. However, the design of most of these MFC controller parameters still takes a trial and error approach, which is time-consuming and expensive. On the other hand, the conventional MFC interpretation framework can approximately hold for systems with slow dynamics but not for systems with fast dynamics, like PE systems. The closed-loop systems designed based on the conventional MFC framework cannot guarantee their performance robustness for mass production.

The objectives of this article are mainly threefold:

1) to gain a systematic understanding of the characteristics of this MFC, which is especially essential for PE systems with fast dynamics;
2) to theoretically benchmark the performance robustness of MFC over the existing control methods, such as linear control methods, revealing that the desired performance robustness can only be obtained with proper design;
3) to generalize the MFC theory for greater robustness, and showcase the potential for achieving PE controller design automation. Particularly, the model-dependent phenomenon of MFC is first reported; a new tool for predicting the stability and dynamic response of an MFC-based closed-loop system is developed; critical comments on the essence of MFC and a new MFC with enhanced performance robustness are included.

II. Review of MFC

This section reviews the principle and interpretation of the "model-free" feature of the conventional MFC based on two assumptions. Then, the limitations of such interpretation for analyzing the true performance of MFC systems especially with PE systems are proposed considering practical issues.

A. Principle of MFC

The basic principle of Fliess's MFC can be explained by considering a single-input-single-output system characterized within its operating range by an ordinary differential equation

$$g_p\left[y(t), y'(t), \ldots, y^{(a)}(t), u(t), u'(t), \ldots, u^{(b)}(t)\right] = 0 \tag{1}$$

where $u(t)$ and $y(t)$ are control input and output at time t, respectively, $a, b \in \boldsymbol{R}$, and $g_p(\cdot)$ is the plant model, being a linear or nonlinear function of $u(t)$, $y(t)$, their higher order derivatives, and external disturbances (not shown in equation).

According to [29], the implementation of MFC involves three steps as follows.

Step 1: Affine model transformation

Transform $g_p(\cdot)$ into an affine form

$$g_p(\cdot) = 0 \rightarrow y^{(v)}(t) = \alpha u(t) + F(t) \tag{2}$$

where α, $v \in \boldsymbol{R}$ are constants, and $F(t)$ can be regarded as a disturbance signal imposed on a linear model $y^{(v)}(t) = \alpha u(t)$.

Step 2: Disturbance signal estimation

From (2), $F(t)$ can be represented as

$$F(t) = y^{(v)}(t) - \alpha u(t). \tag{3}$$

Thus, $F(t)$ can be estimated without knowing $g_p(\cdot)$ via an algebraic observer, which is a variation of (3)

$$\hat{F}(t) = y^{(v)}(t) - \alpha u(t - T_s) \tag{4}$$

where $u(t–T_s)$ is the system input in the last time step to avoid an algebraic loop in practice, and $\hat{F}(t)$ is an estimate of $F(t)$.

From (3) and (4), provided that $u(t)$ is continuous in time and that sampling time $T_s \to 0$, then $u(t) \approx u(t-T_s)$ so that $F(t)$ can be well estimated by

$$F(t) \approx \hat{F}(t). \tag{5}$$

Step 3: Feedback linearization control

With the estimated $F(t)$ and the affine model (2), a controller $u(t)$ based on feedback linearization can be devised

$$u(t) = \frac{-\hat{F}(t) + y_r^{(v)}(t) + g_c[e(t)]}{\alpha} \tag{6}$$

where $y_r(t)$ is the reference signal of $y(t)$, $e(t) = y_r(t) - y(t)$ the reference tracking error, and $g_c(\cdot)$ a causal function of $e(t)$.

Combining (3), (5), (6) leads to an error dynamics of

$$e^{(v)} + g_c[e(t)] = 0. \tag{7}$$

The desired steady state and dynamic performance can then be achieved via a proper design of $g_c(\cdot)$. Similar MFC principles also apply to multiple-input-multiple-output (MIMO) systems [14], [30], [31].

B. Existing MFC Interpretation

From (6) and (7), one can see that a system with MFC appears to result in model-independent closed-loop dynamics and stability performance. Such feature of MFC suggests the possibilities of

1) *Model-free design:* The dynamics and stability performance of a system with MFC can be precisely controlled through the design of $g_c(\cdot)$ only, requiring no knowledge of $g_p(\cdot)$.
2) *Model-free operation:* The dynamics and stability performance of a system with MFC is perfectly robust against model $g_p(\cdot)$ variations.

These desirable properties readily differentiate MFC from model-based control methods, including linear control and model-predictive control, etc., the design of which typically necessitates the knowledge of $g_p(\cdot)$ while perfect robustness cannot be achieved. On the other hand, MFC also differs from most other types of model-free control methods reported in the literature, such as the model identification adaptive control, artificial intelligence-based control, etc., since they generally demand: 1) a large dataset which may be unavailable, and 2) a high-performance computing unit to be added to the system [32]. MFC, in contrast, can be dataset and computation light. For example, according to (4) and (6), if $v = 1$, $g_c(\cdot)$ is proportional to $e(t)$, i.e., $g_c(\cdot) = ke(t)$, and the controller is discretized by the backward Euler method, the associated MFC control law is

$$u(t) = u(t - T_s) + \left(\frac{1}{\alpha T_s} + \frac{k}{\alpha}\right) e(t) - \frac{1}{\alpha T_s} e(t - T_s). \tag{8}$$

Clearly, the controller implementation only needs 1) the data of $y(t)$, $y(t–T_s)$, $y_r(t)$, $y_r(t–T_s)$, and $u(t–T_s)$ and 2) four addition and two multiplications.

C. Limitations of Existing MFC Interpretation

MFC has found tremendous applications both in the literature and in the field due to its possibility for model-free design and operation. The existing MFC interpretation says that the model-free properties hold given the premises that $u(t) \approx u(t-T_s)$ holds and that $y^{(v)}(t)$ can be estimated accurately. There are, however, three key challenges and issues in a practical setting:

1) $T_s \to 0$ may not be satisfied practically. Most reported work on MFC is based on digital implementations with $T_s >> 0$. On the other hand, even if $T_s \to 0$ can be physically achieved, e.g., through analog implementation, instability might occur, as will be explained in Section IV.
2) $u(t)$ may be discontinuous in time. Most reported work on MFC tested abrupt model variations (e.g., a step load change in a PE system [18]) and/or the control law contains a differentiator term from the reference signal; thus, $u(t)$ in (6) becomes a discontinuous function of t.
3) The term $y^{(v)}(t)$ in (4) in most literature is calculated by numerical differentiation, often implemented with an extra low-pass filter (LPF) stage to filter out the noise [33], i.e., $y^{(v)}{}_{\text{calculated}}(t) = D[y^{(v)}(t)]$, where $D(\cdot)$ is a function due to discretization, quantization, and/or LPF. For example, the original estimation of $F(t)$ is made possible by approximating $F(t)$ as a piecewise constant function updated based on algebraic identification techniques [29]. This technique can effectively average $y^{(v)}(t)$ within a time window, allowing for greater noise rejection capability than the direct differentiation operation. The averaging function is in effect an LPF as proved by [34], resulting in a substantial estimation error of $F(t)$, especially in the medium- and high-frequency domain. Some reported work aims to find a "good" estimation of $F(t)$, either through increasing sampling frequency or increasing estimation accuracy by combining with advanced observers, including extended state observer (ESO) [35], [36], sliding mode observer (SMO) [15], [37], etc., also with input compensators such as fuzzy logic [37], neural network [38], etc., which can effectively improve the system performance to some extent. However, most of them 1) are asymptotic estimation techniques thus the closed-loop stability margin may be reduced, and 2) add the controller's complexity, losing the original MFC's advantage of simple structure and low computational cost; 3) the estimation error between practice and theory always exists due to unavoidable measurement noise and environmental disturbances. Therefore, $F(t) \neq \hat{F}(t) = y^{(v)}{}_{\text{calculated}}(t) - \alpha u(t–T_s)$, even if $T_s \to 0$ and $u(t)$ is a continuous function of t.

Due to the reasons above, MFC might lose the model-free properties in a practical setting. Specifically, these challenges become more severe for systems with extremely fast dynamics, such as PE systems. Thus, the original MFC understanding is insufficient for analyzing the performance of such systems. The crucial question now is how to characterize and benchmark the *true* performance of MFC with arbitrary T_s and $\hat{F}(t)$ and whether the model-free features still hold.

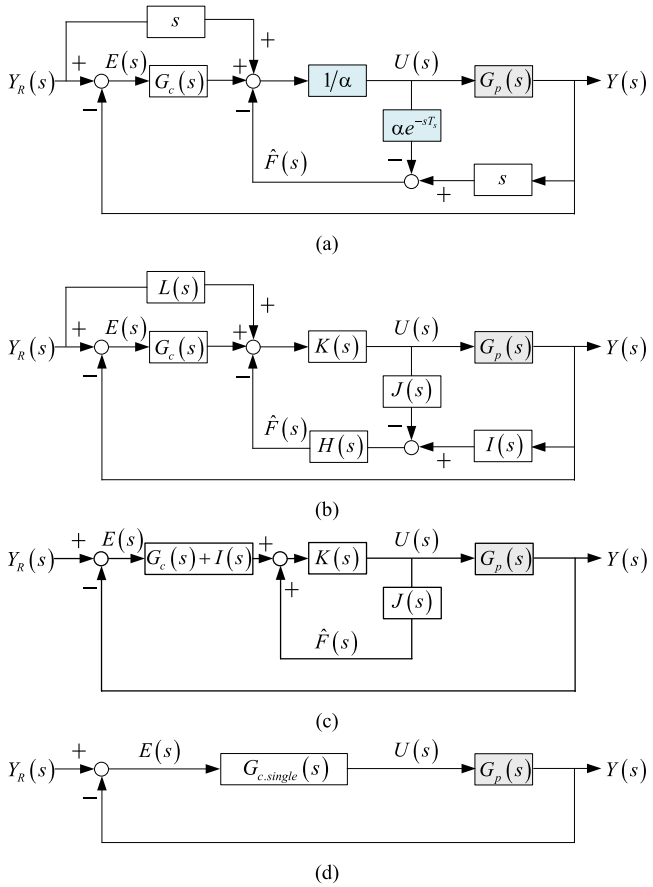

Fig. 2. Control diagram of (a) conventional MFC with $H(s) = 1$; (b) generalized MFC; (c) MFC with $H(s) = 1$ and $L(s) = I(s)$; (d) single-loop feedback control.

III. MFC Revisited

In this section, we apply the classical control theory, i.e., using the Laplace transform as a basic tool, to revisit MFC. We will show that an MFC-controlled system may lose the model-free properties in practice but may achieve robust quasi-model-free design and operation (i.e., only the knowledge of the nominal plant model is needed).

A. Essence of MFC

According to (2)–(6), a MFC system can be described by an s-domain control diagram in Fig. 2(a). Here, for the ease of presentation, $v = 1$, a common choice in the literature [39], is assumed for the affine model, where $G_p(s)$, $U(s)$, $Y(s)$, $Y_R(s)$, $E(s)$, $\hat{F}(t)$, and $G_c(s)$ are the Laplace transform of $g_p(\cdot)$, $u(t)$, $y(t)$, $y_r(t)$, $e(t)$, $\hat{F}(t)$, and $g_c(\cdot)$, respectively, and e^{-sTs} denotes the unit delay in (4).

Structurally speaking, Fig. 2(a) shows that the existing MFC is essentially a special form of cascaded control (or minor loop feedback control) [40] with only one feedback signal. This cascaded control is different from the conventional cascaded control (e.g., consisting of an outer PI voltage loop and an inner PI current loop) used in many power electronics converters where two feedback signals are needed (e.g., a voltage and a current signal). Specifically, the output of the outer-loop controller $G_c(s)$ provides the reference signal for the inner-loop controller, consisting of proportional controller $1/\alpha$, a feedback network s, and a feedforward term αe^{-sTs}. By extending the cascaded control concept, a generalized MFC control diagram can be formulated in Fig. 2(b), where $I(s)$, $H(s)$, $J(s)$, and $K(s)$ are the transfer functions along the four branches of the inner control loop and $L(s)$ is a feedforward term of the reference signal. The corresponding s-domain affine model is

$$Y(s)\,I(s) = J(s)\,U(s) + H^{-1}(s)\,F(s). \tag{9}$$

TABLE I
Configurations of Several MFC Methods

Control method	Outer loop Controller		Inner loop Controller			
	G_c	L	I	K	J	H
MFC-1	k	0	s	$1/\alpha$	$\alpha s e^{-sTs}$	1 or LPF
i-P		s				
i-PI	$k_p + k_i/s$	s or s^2	s or s^2			1
i-PID	$k_p + k_i/s + k_d s$					
MFSMCS	Sliding mode control	s	s			
MFC-DPC	Deadbeat control	s^2	s^2			
MFC-NIB	Nonlinear integral backstepping control					
MFC-2	k	0	s	$1/\beta s$	$\beta s e^{-sTs}$	1 or LPF

Different combinations of $I(s)$, $K(s)$, $H(s)$, and $J(s)$ will lead to different affine models for MFC implementation. Table I illustrates several examples, including some previously reported MFC methods along with their respective outer and inner-loop configurations, such as the intelligent proportional (i-P) [41], intelligent-PI (i-PI) [18], [42], intelligent-PID (i-PID) controller [16], [17], [43], [44], model-free sliding mode control system (MFSMCS) [45], model-free-control based deadbeat predictive control (MFC-DPC) [46], and model-free control based nonlinear integral backstepping control (MFC-NIB) [47]. Table I shows that the existing MFC methods are almost identical in terms of their corresponding affine models, the linear portion of which is invariably $y^{(v)}(t) = \alpha u(t)$. Instead of studying these MFC methods individually, the following discussions will focus on the generalized MFC based on Fig. 2(b). The objective is to obtain a systematic understanding of MFC's characteristics, thus to characterize the true performance of PE systems controlled by MFC.

B. Dynamics and Stability

To analyze the dynamics and stability characteristics of MFC and show the model-dependent feature of MFC, the closed-loop transfer function of the system shown in Fig. 2(b) can be expressed as

$$\frac{Y(s)}{Y_R(s)} \triangleq G_{cl.MFC}(s) = \frac{(G_c(s) + L(s))\,G'_p(s)}{1 + (G_c(s) + L(s))\,G'_p(s)} \tag{10}$$

where

$$G'_p(s) = \frac{1}{I(s)\,H(s) - L(s)} \frac{T(s)}{1 + T(s)} \tag{11}$$

is the closed-loop transfer function of the inner loop, and

$$T(s)=\frac{K(s)(I(s)H(s)-L(s))}{1-H(s)K(s)J(s)}G_p(s) \tag{12}$$

is the inner loop gain.

In particular, when $H(s)=1$ and $L(s)=I(s)$, as many existing MFC methods do (see Table I), one obtains $T(s)=0$, meaning that the dual-loop control system effectively reduces to a single-loop control system. In this case, the closed-loop dynamics can still be characterized by (10), and (11) becomes

$$G'_p(s)=\frac{K(s)}{1-K(s)J(s)}G_p(s) \tag{13}$$

and an equivalent control block diagram is shown in Fig. 2(c). For example, when $H(s)=1$, $L(s)=I(s)=s$, and $G_c(s)=k$ (i-P in Table I with $H(s)=1$), MFC implemented in discrete time domain will be identical to a discrete PI controller [48] as shown in (8).

Equations (10)–(12) can thus provide a powerful tool for characterizing the dynamic performance and stability of the system for arbitrary T_s and $\widehat{F}(t)$ by, e.g., identifying the poles and zeros of the system. It is also shown that the dynamics and stability of a system with MFC are functions of not only $G_c(s)$ but also the plant model $G_p(s)$ and inner-loop terms, including the filter term $H(s)$. In other words, MFC is essentially a model-based controller in the sense that

1) *Model-based design:* The dynamic performance and the stability of a system with MFC are *not* solely determined by $g_c(\cdot)$. Some knowledge of $g_p(\cdot)$ is essential.
2) *Model-based operation:* A closed-loop system with MFC is not perfectly robust, i.e., the dynamics and stability will be affected by $g_p(\cdot)$ variations.

The following analysis will focus on the case when MFC is equivalent to a cascaded controller. An MFC with $H(s)=1$ and $L(s)=I(s)$ is effectively identical to a single-loop linear controller, thus will be regarded as a type of single-loop linear controller hereafter.

C. Performance Robustness

Despite being model-dependent, MFC with a cascaded control structure is found possible to be extraordinarily performance robust against model variations as compared to most existing control methods, which generally have a single-loop control structure.

To illustrate this, the system sensitivity $S_{G_p}^{\ G_{cl}}$ analysis is performed over a single loop and a cascaded control structure, respectively. $S_{G_p}^{\ G_{cl}}$ measures the ratio between the relative change in the closed-loop transfer function $G_{cl}(s)$ and that in the plant model $G_p(s)$ in the sense of small signal [1]. A lower $S_{G_p}^{\ G_{cl}}$ at the bandwidth frequency f_{BW} means more performance robust, and vice versa.

The $S_{G_p}^{\ G_{cl}}$ of a general single-loop linear control system [see Fig. 2(d)] is known to be [1]

$$S_{G_p}^{G_{cl.single}}=\frac{\partial G_{cl.single}}{\partial G_p}\cdot\frac{G_p}{G_{cl.single}}=\frac{1}{1+G_{c.single}(s)G_p(s)} \tag{14}$$

where $G_{c.single}(s)$ is the single-loop controller, and

$$G_{cl.single}(s)=\frac{G_{c.single}(s)G_p(s)}{1+G_{c.single}(s)G_p(s)} \tag{15}$$

is the $G_{cl}(s)$ of the single-loop control system.

On the other hand, from (10)–(12), one can obtain $S_{G_p}^{\ G_{cl}}$ of a generalized MFC system as

$$S_{G_p}^{G_{cl.MFC}}=\frac{\partial G_{cl.MFC}}{\partial G_p}\cdot\frac{G_p}{G_{cl.MFC}}=\frac{\frac{1}{1+T(s)}}{1+(G_c(s)+L(s))G'_p(s)}. \tag{16}$$

From (14) and (16), and provided that both control structures have identical $G_{cl}(s)$ at the nominal $G_p(s)$, i.e., $G_{c.single}(s)G_p(s)=(G_c(s)+L(s))G'_p(s)$, one obtains

$$\frac{S_{G_p}^{G_{cl.MFC}}}{S_{G_p}^{G_{cl.single}}}=\frac{1}{1+T(s)}. \tag{17}$$

Equation (17) suggests that the performance robustness of MFC is $1+T(s)$ times that of a single-loop controller for a given identical control bandwidth, i.e., at f_{BW}, if $\|1+T(s)\|>1$, the performance robustness can be improved by MFC, and vice versa. In the extreme case of $\|1+T(s)\|>>1$ at f_{BW}, (10) and (11) can be approximately expressed as

$$G'_p(s)\approx\frac{1}{I(s)H(s)-L(s)} \tag{18}$$

$$G_{cl.MFC}(s)\approx\frac{G_c(s)+L(s)}{G_c(s)+I(s)H(s)} \tag{19}$$

which are independent of the plant model $G_p(s)$. Performance robustness is thus a key feature of MFC.

It should be emphasized that

1) this robust property of MFC can be uniquely attributed to the cascaded control structure, which offers a new dimension to tune the system robustness (or sensitivity) via the design of $T(s)$, including the configurations of terms $I(s)$, $L(s)$, $H(s)$, $J(s)$, and $K(s)$;
2) the model-free operation suggested by (19) may not be achievable in practice, as the system might become unstable when $\|1+T(s)\|>>1$ (see explanations in Section IV-A);
3) however, if we can design MFC such that $\|1+T(s)\|$ is sufficiently large while still ensuring the system stability, the system should tolerate significant model variations while retaining a $G_{cl}(s)$ close to that at the nominal plant model $G_p(s)$, achieving *quasi-model-free* design and operation.

IV. Derivation of New MFC

Through the generalized framework provided in Section III, the limitations of stability and performance robustness of conventional MFC are analyzed, and new derivatives of MFC that can achieve quasi-model-free design and operation are reported.

A. Limitations of Conventional MFC

Although potentially being more performance robust than single-loop controllers, the conventional MFC is found to have

an upper bound to $\|1+T(s)\|$, which limits its capability to achieve greater performance robustness.

To show such limitations, we substitute the inner-loop transfer functions of the conventional *i*-P type MFC in Table I into (12) and obtain

$$T_{i-P}(s)=\frac{s\left(H(s)-1\right)G_p(s)}{\alpha\left(1-H(s)\,e^{-sT_s}\right)}. \tag{20}$$

Equation (20) shows that there is a high-pass filter (HPF) term ($H(s)$ - 1) in the inner loop gain, which tends to amplify $T_{i\text{-}P}(s)$ in the high frequency ranges. This amplification in the high frequency ranges may decrease the stability margin of the inner loop and thus that of the overall system. Thus, the low-frequency gain of $\|1+T(s)\|$ needs to be sufficiently small to ensure stable system operation. A small $\|1+T(s)\|$, however, suggests a relatively poorer system robustness. Thus, we propose to substitute the inner-loop transfer functions of the conventional *i*-P type MFC with $L(s)=0$ (MFC-1 hereafter) in Table I into (12) and obtain

$$T_{MFC1}(s)=\frac{sH(s)\,G_p(s)}{\alpha\left(1-H(s)\,e^{-sT_s}\right)}. \tag{21}$$

Compared with (20), (21) shows that $\|T_{MFC1}(s)/\,T_{i\text{-}P}(s)\| \to 0$ when $\omega\to\infty$, which is beneficial to improving the stability margin of the system. With the small T_s approximation

$$T_{MFC1}(s)\approx\begin{cases}\frac{G_p(s)}{\alpha T_s}, & H(s)=1\\ \frac{G_p(s)}{\alpha\left(T_s+\frac{1}{\omega_c}\right)}, & H(s)=\frac{\omega_c}{\omega_c+s}\end{cases}. \tag{22}$$

Here, $H(s)=1$ and $H(s)=\omega_c/(s+\omega_c)$ refer to the cases without filter and with a first-order LPF, respectively.

Equation (22) shows that $\|1+T_{MFC1}(s)\|\to\infty$ can be achieved in the case of no filter provided that $T_s\to 0$ and/or $\alpha\to 0$, which is beneficial for obtaining high performance robustness. This conclusion aligns with the premises of demanding $T_s\to 0$ and $H(s)=1$ to realize model-free operation as mentioned in Section II.

However, an excessively small T_s and/or α may lead to stability concerns, as the resultant inner-loop gain $\|T_{MFC1}(s)\|$ will be amplified uniformly at all frequencies, as per (22). A larger loop gain in the higher frequency ranges is a well-known cause of system instability [49]. Thus, T_s and/or α need to be sufficiently large to maintain a low $\|T_{MFC1}(s)\|$ at higher frequencies to keep the system stable, leading to a lower $\|1+T_{MFC1}(s)\|$ and thus lower performance robustness.

Equation (22) also shows that $\|1+T_{MFC1}(s)\|\to\infty$ cannot be achieved even if $T_s\to 0$ when $H(s)\neq 1$ (in the case with a first-order filter), which is more practical. Additionally, a sufficiently large α is required to ensure the system stability for a similar reason above, leading to a lower $\|1+T_{MFC1}(s)\|$.

To improve the performance robustness of MFC-1, a new MFC, known as MFC-2, is proposed below. The idea is to reconfigure the inner-loop terms of Fig. 2(b) to elevate the magnitude of $\|1+T(s)\|$ nonuniformly, i.e., only in the lower frequency ranges. Despite that perfect robustness (i.e., $\|1+T(s)\|\to\infty$) may still not be obtainable, MFC-2 can sufficiently boost $\|1+T(s)\|$ below f_{BW} while ensuring the system stability to achieve *quasi-model-free* design and operation.

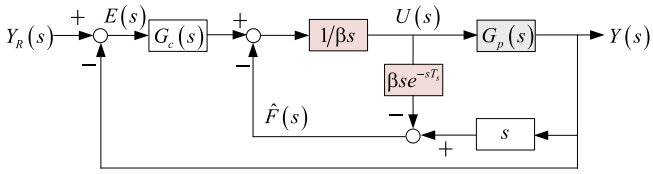

Fig. 3. Control diagram of MFC-2 with $H(s)=1$.

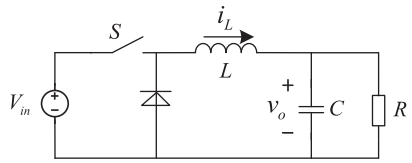

Fig. 4. Circuit topology of a buck converter.

B. New MFC

From (12), we replace α in MFC-1 with βs to formulate MFC-2, and obtain new $I(s)$, $J(s)$, and $K(s)$ designs as tabulated in the last row of Table I. This leads to an inner-loop gain as

$$T_{MFC2}(s)=\frac{H(s)\,G_p(s)}{\beta\left(1-H(s)\,e^{-sT_s}\right)}. \tag{23}$$

Compared to (21), the "s" term in the numerator of $T_{MFC2}(s)$ is eliminated. With a small T_s approximation, we obtain

$$T_{MFC2}(s)\approx\begin{cases}\frac{G_p(s)}{s\beta T_s}, & H(s)=1\\ \frac{G_p(s)}{s\beta\left(T_s+\frac{1}{\omega_c}\right)}, & H(s)=\frac{\omega_c}{\omega_c+s}\end{cases}. \tag{24}$$

Equation (24) shows that for an arbitrary $G_p(s)$ containing no zeros at the origin, even with a large T_s and/or β, $\|1+T_{MFC2}(s)\|\to\infty$ when $\omega\to 0$ and $\|1+T_{MFC2}(s)\|\to 0$ when $\omega\to\infty$. The large $\|1+T_{MFC2}(s)\|$ at low-frequency ranges is expected to enhance the system performance robustness.

The control diagram of MFC-2 with $H(s)=1$ is shown in Fig. 3, and the corresponding affine model is

$$sY(s)=s\beta U(s)+F(s) \tag{25}$$

in the s-domain, or

$$\frac{dy(t)}{dt}=\beta\frac{du(t)}{dt}+F(t) \tag{26}$$

in the time domain.

By following the same principle, it is possible to develop other MFC methods for enhanced performance robustness. However, (12) suggests that there is no universal MFC loop term configuration that fits all $G_p(s)$ for enhanced robustness. Instead, the optimal MFC configuration must be customized as per $G_p(s)$, which is usually the best estimate of the plant's nominal model.

V. Comparative Studies

A buck converter, as shown in Fig. 4, is used as an example to further evaluate the performance of MFC in PE applications through a comparative study of the following four control methods: (a) single-loop PI control, (b) MFC-1, (c) MFC-2, and (d) *i*-P.

TABLE II
SYSTEM PARAMETERS

Parameters	Nominal (Tested) Values
V_{in}	24 V (16.8– 31.2V)
V_o	12 V
L	1 mH (0.2– 5 mH)
C	1 μF (0.2– 5 μF)
R	15 Ω (3– 75 Ω)
T_s	10 μs (f_s = 100 kHz)
ω_c	113 097 rad/s

TABLE III
CONTROLLER PARAMETERS

Control method	Parameters	Values	
		Model variation space 1	Model variation space 2
PI	[k_p, k_i]	[0.01, 36]	[0.01, 37]
MFC-1.a	[α, k]	[2082580, 2000]	[477020, 1080]
MFC-1.c	[α, k]	[-3092585, -1040]	[-3092585, -1040]
MFC-2	[β, k]	[250, 703]	[67, 768]
i-P	[α, k]	[2353900,1920]	/

The state-space averaged plant model of a buck converter is

$$G_p(s) = \frac{V_o(s)}{U(s)} = \frac{V_{in\_n}}{L_n C_n s^2 + \frac{L_n}{R_n} s + 1} \tag{27}$$

where V_{in_n}, L_n, C_n, and R_n are the nominal input voltage, inductance, capacitance, and load resistance, and V_o (s) and $U(s)$ the Laplace transform of the output voltage $v_o(t)$ and the duty cycle $u(t)$ of the active switch S, respectively. Both cases with and without an LPF are studied. To be consistent with the experiments for performance validation, the following studies will be conducted in the z-domain as the experiments will be based on microcontroller implementations. Unless otherwise indicated, the nominal circuit parameters in Table II and the controller parameters based on model variation space 1 in Table III are used. All the controller parameters are calculated based on Pareto front analysis in Section V-D.

A. Model Dependencies

To verify that both stability and dynamics of MFC are model-dependent whether $H(s)$ is a low-pass filter or not, several root locus analysis and simulation results based on MFC-1 as an example are reported below.

Figs. 5 and 6 illustrate the root loci of the buck converter system controlled by MFC-1 with an LPF (noted as MFC-1.a) as a function of (a) R and (b) α, respectively. In both cases, the location of the dominant pole (D-pole) varies with R and α, leading to variation in system dynamics. Additionally, as α decreases and/or R increases, several higher frequency poles tend to be outside of the unit circle, leading to system instability. These observations confirm that MFC cannot achieve model-free design and operation if an LPF is applied even with a small $T_s = 10$ μs. Instead, the dynamics and stability rely on the plant parameters and inner-loop gain $T(s)$, simultaneously.

The results also confirm that the inner loop gain $T(s)$, which is inversely proportional to α, should remain sufficiently low. For instance, in Fig. 6, the poles with α (low $T(s)$ case) will lead to a stable operation while the poles with $\alpha/8$ (high $T(s)$ case) will lead to unstable operation.

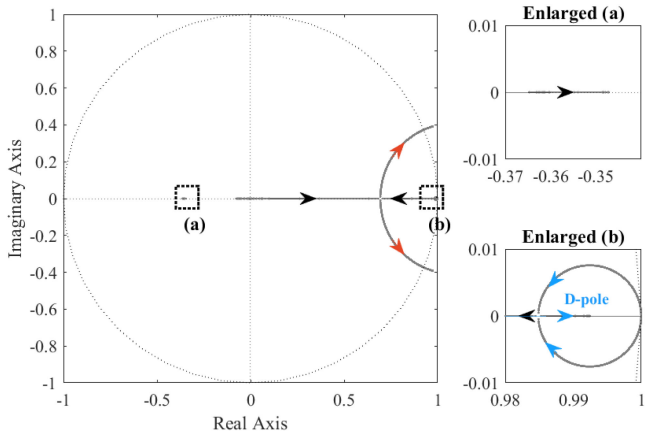

Fig. 5. Root locus of the buck converter system controlled by MFC-1.a as R increases.

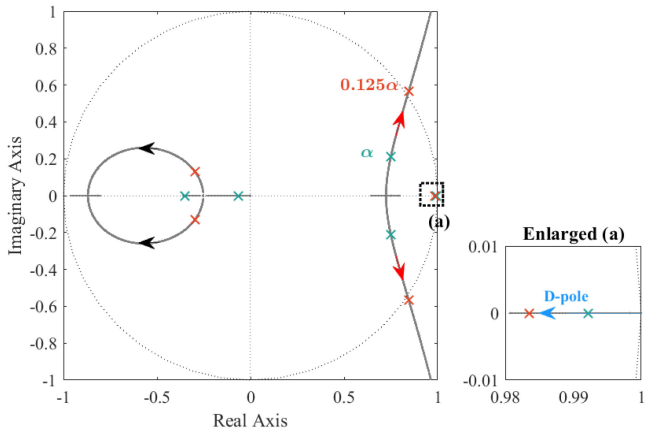

Fig. 6. Root locus of the buck converter system controlled by MFC-1.a as α decreases.

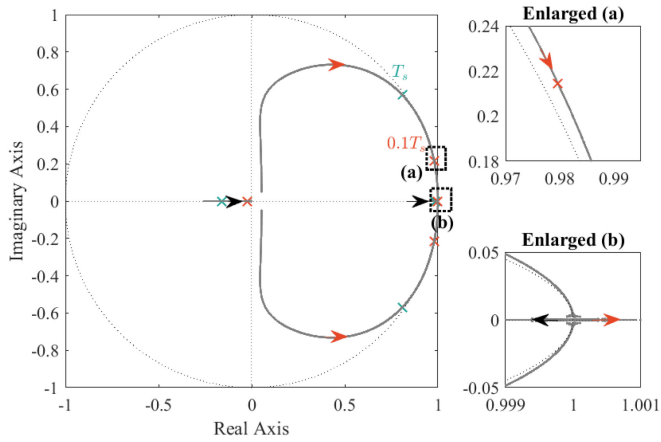

Fig. 7. Root locus of ideal MFC-1.b system as T_s decreases.

Fig. 7 shows the root locus of buck converter controlled by MFC-1 in the no filter case with $H(s) = 1$ (noted as MFC-1.b) as a function of T_s. The controller parameters are $[\alpha, k] = [499650, 2000]$. As T_s decreases, there are poles that tend to be outside of the unit circle, leading to system instability. For instance, in

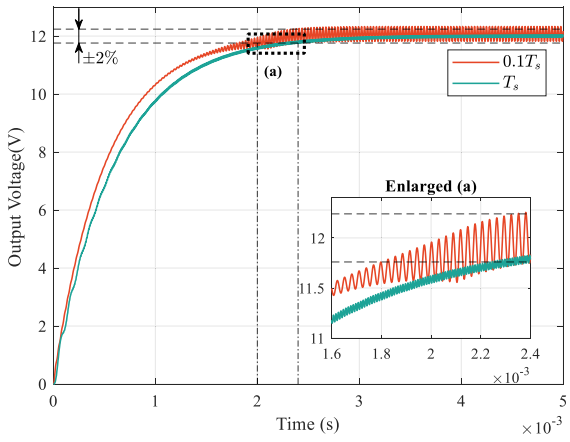

Fig. 8. Simulation results of output voltage step response controlled by MFC-1.b with T_s variation.

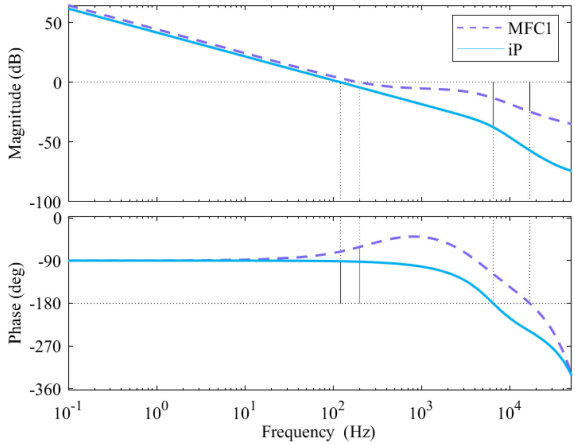

Fig. 9. Bode plots of open-loop transfer function under MFC-1.a and *i*-P.

Fig. 7, the poles with $T_s = 10$ μs (low $T(s)$ case) will lead to a stable operation while the poles with $T_s/10$ (high $T(s)$ case) will lead to unstable operation. This means that the system cannot achieve $T_s \to 0$ in theory. The model-free operation and design as illustrated by (7) cannot be achieved in the case of no filters. Therefore, MFC-1 and MFC-2 in the following study are designed with a first-order LPF for $H(s)$.

To further illustrate the effects of T_s on system stability, the corresponding simulation of buck converter controlled by MFC-1.b is conducted by PSIM simulation software. Fig. 8 shows the step responses of v_o when its reference v_o^* changes from 0 V to 12 V with different T_s. These waveforms confirm that a small T_s (i.e., $T_s/10$) can cause system instability while a large T_s can enhance the system stability.

B. Stability Margin Comparison of MFC-1 and i-P With LPF

To show the impact of feedforward path $L(s)$ on the system, the stability margins of the open-loop transfer functions of MFC-1 and *i*-P are compared in Fig. 9. Both controllers are shown in model variation space 1 in Table III, which are designed via the Pareto front in Section V-D. It is shown that although *i*-P

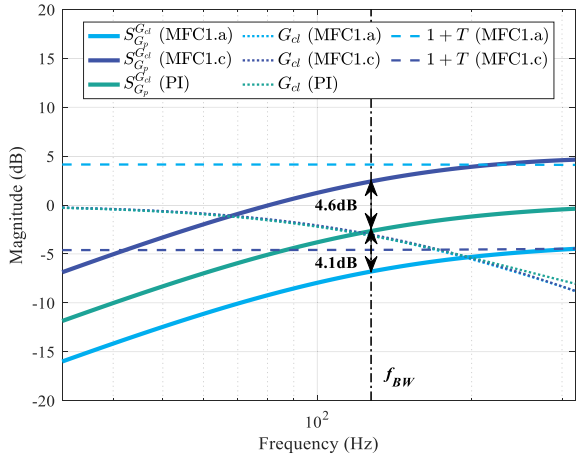

Fig. 10. Bode plots of system inner-loop gain, sensitivity, and closed-loop transfer function with PI, MFC-1.a, and MFC-1.c control.

obtains a bit higher bandwidth, it has less gain margin than MFC-1, which may have an adverse impact on stability considering model variation.

C. Comparisons of System Sensitivities

To make a theoretical comparison in terms of performance robustness of MFC-1, MFC-2, and PI, system sensitivities are compared:

1) Single-loop controller and MFC: Two MFC-1 controllers (MFC-1.a and MFC-1.c, both with LPF) and one PI controller are further evaluated. All controllers are designed with almost identical $G_{cl}(s)$ below f_{BW} (see dotted lines in Fig. 10). Additionally, MFC-1.a is designed with $\|1 + T(s)\| = 4.1$ dB > 1 at f_{BW}, and MFC-1.c with $\|1 + T(s)\| = -4.6$ dB < 1 at f_{BW}. Fig. 10 shows that MFC-1.a can lower $S_{G_p}^{G_{cl}}(s)$ by 4.1 dB (i.e., 1.6-fold) compared to that of the PI controller at f_{BW}, while MFC-1.c does the opposite. These observations are a good match to (17), highlighting the capabilities of MFC methods in improving performance robustness and the importance of having a $\|1 + T(s)\| > 1$ design.
2) MFC-1 and MFC-2: A MFC-2 controller is further designed with almost identical $G_{cl}(s)$ below f_{BW} to that of PI and MFC-1.a above. From Fig. 11, the following can be observed: (i) $\|1+T(s)\|$ of MFC-2 exhibits a –20 dB/dec slope while that of MFC-1.a is almost constant across a broad frequency band, and (ii) MFC-2 can achieve a much greater $\|1+T(s)\|$ at and below f_{BW} than MFC-1.a. These are expected results from Section IV. At f_{BW}, MFC-2 shows a $S_{G_p}^{G_{cl}}(s)$ of 14.6 dB lower than that of MFC-1.a, meaning that the performance robustness of MFC-2 is 5.4 times that of MFC-1.a and 8.6 times that of PI controller.

D. Pareto Fronts Comparison

To enable a more comprehensive and systematic comparison of performance robustness, a Pareto front analysis is performed over PI, MFC-1, MFC-2, and *i*-P, to achieve optimal robust performance. There is some knowledge of $g_p(\cdot)$ needed in the

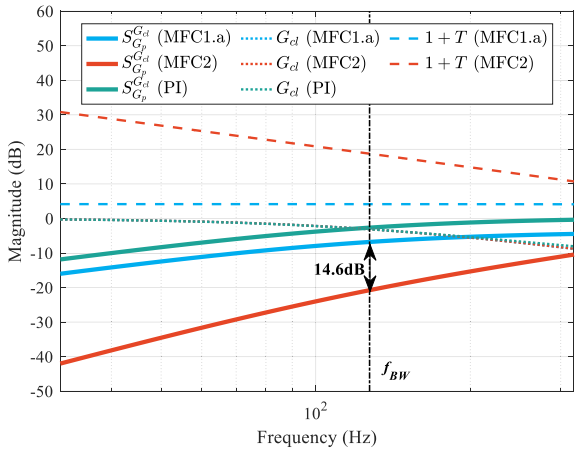

Fig. 11. Bode plots of system inner loop gain, sensitivity, and closed-loop transfer function under MFC-1.a, PI control, and MFC-2.

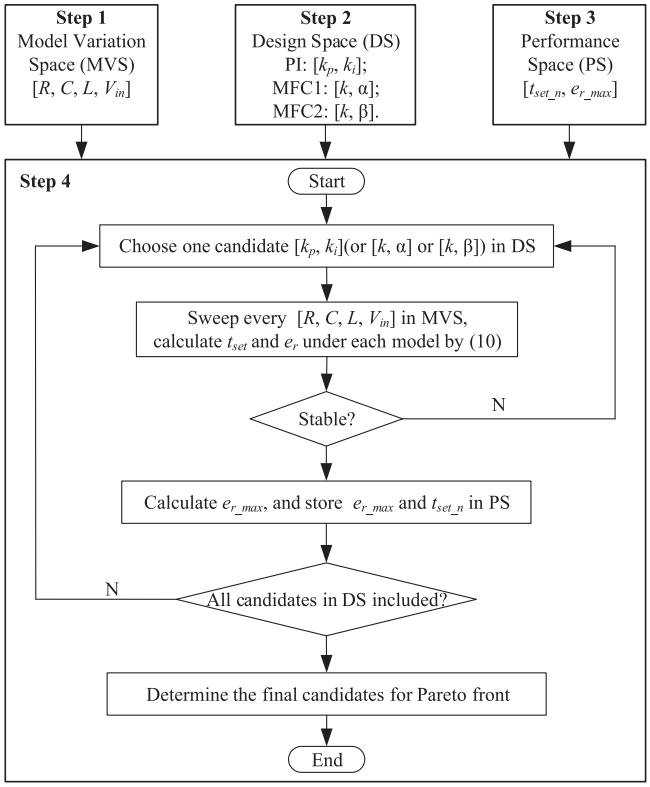

Fig. 12. Flowchart of Pareto front design for PI, MFC1, and MFC2.

design stage: i) the best estimate of the plant's nominal model and ii) assumptions about the model uncertainties. A design procedure similar to that in [50] is adopted. Fig. 12 depicts the design flowchart for optimal performance robustness, with the detailed design procedure.

Step 1: Construct model variation spaces

Two model variation spaces are evaluated in this article.

i) Model variation space 1: [R, C, L, V_{in}] = [R_n, C_n, L_n, V_{in_n}]· (diag [i, 1, 1, 1] ∪ diag [1, i, 1, 1] ∪ diag [1, 1, i, 1]), where 20% ≤ i ≤ 500%, corresponding to ±5-fold variations of circuit parameters R, C, and L. (The controller parameters of i-P is only explored for model variation space 1 to show the stability considering R variation.)

ii) Model variation space 2: [R, C, L, V_{in}] = [R_n, C_n, L_n, V_{in_n}] diag [1, 1, 1, i], where 70% ≤ i ≤ 130%, corresponding to ± 30% variations of the operating point, V_{in}.

Step 2: Formulate controller design spaces

i) Design space for PI: $10^{-4} \le k_p \le 10^{-1}$, $10 \le k_i \le 10^3$.

ii) Design space for MFC-1 (i-P): $10^2 \le k \le 10^5$, $10^4 \le \alpha \le 10^7$.

iii) Design space for MFC-2: $10 \le k \le 10^5$, $10 \le \beta \le 10^3$.

Step 3: Setup performance spaces

The performance space is selected as [t_{set_n}, $e_{r\cdot max}$], where t_{set_n} is the settling time (a measurement of the system dynamic performance under nominal conditions) of a closed-loop system with nominal model parameters, i.e., [R_n, C_n, L_n, V_{in_n}], in the presence of a step-change in the voltage reference signal, and $e_{r\cdot max}$ is the maximum relative t_{set} error as a result of model variation, which is defined as $e_{r\cdot max} = \max |t_{set} - t_{set\_n}| / t_{set\_n}$ and used to measure performance robustness.

Step 4: Explore the design space and output Pareto fronts.

The controller design space is thoroughly explored, and each controller candidate is evaluated within the model variation space regarding e_r, t_{set}, and stability based on our new modeling tool (10). For each t_{set_n}, the optimal control parameters that can achieve minimum $e_{r\cdot max}$ over the model variation space are then determined. The associated t_{set_n} and $e_{r\cdot max}$ are finally recorded, formulating the Pareto fronts.

Fig. 13 shows the Pareto fronts of the four controllers within model variation space 1. The following four key observations can be made:

1) Both MFC-1 and MFC-2 can achieve a lower $e_{r\cdot max}$ than the PI controller when $t_{set\_n} > 4$ ms. This confirms that the MFC controllers can be design more performance robust than the PI controller. Here, the controller parameters at points A1–A3 of Fig. 13 correspond to the PI,

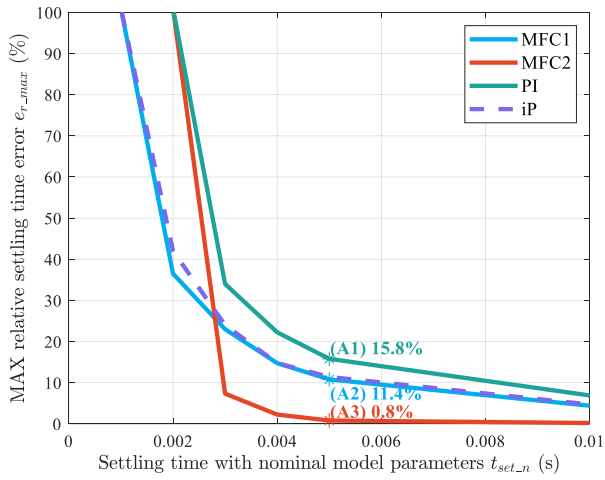

Fig. 13. Pareto fronts for model variation space1 (±5 times *RCL* variation).

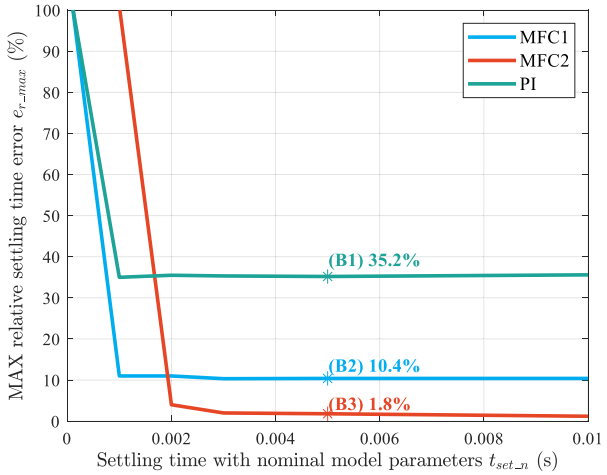

Fig. 14. Pareto fronts for model variation space2 (±30% V_{in} variation).

MFC-1.a, and MFC-2 discussed in Sections V-A and V-C above.

2) MFC-2 can achieve a lower $e_{r\cdot max}$ than MFC-1 when $t_{set\_n} > 4$ ms. This is also an expected result from the sensitivity comparisons in Fig. 11. Specifically, Fig. 13 predicts that MFC-2 can consistently achieve $e_{r\cdot max} < 2\%$, despite more than an order of magnitude (25-fold) of circuit parameter variations. The negligible $e_{r\cdot max}$ suggests that quasi-model-free design and operation based only on the nominal plant model instead of the true plant model is possible.
3) $e_{r\cdot max}$ of all three controllers sharply increases as $t_{set\_n} <$ 4 ms. This phenomenon is mainly attributed to a decreased stability margin at higher f_{BW}. To remain stable, MFC needs to be designed with a lower $\|T(s)\|$, resulting in a reduced $\|1+T(s)\|$, which lowers the performance robustness.
4) MFC can achieve a faster reference tracking speed given the same $e_{r\cdot max}$ constraint. For instance, if a design specification demands $e_{r\cdot max} < 10\%$ with respect to model variation space 1, then MFC-2 can achieve $t_{set\_n} = 2$ ms, MFC-1 5ms, and PI 8ms.
5) i-P and MFC-1 can achieve a similar $e_{r\cdot max}$ at all t_{set_n}, which indicates eliminating the feedforward path in the generalized MFC does not deteriorate its performance robustness.

The above results indicate that MFC can yield all-around improvements regarding both operating bandwidth and performance robustness.

Fig. 14 further shows the Pareto fronts of PI, MFC-1, and MFC-2 within model variation space 2. Again, PI is shown to be the most performance sensitive while MFC-2 is the most robust. Simultaneous improvements in the operating bandwidth and robustness with MFC are evident. The controller parameters at points A1–A3 in Fig. 13 (for model variation space 1) and B1–B3 in Fig. 14 (for model variation space 2) are recorded in Table III and will be used in Section VI in experiments.

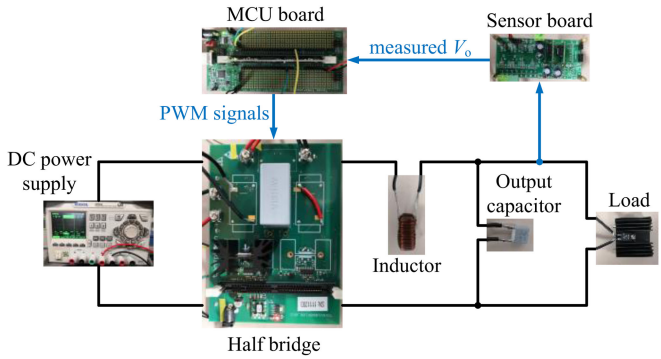

Fig. 15. Buck converter prototypes.

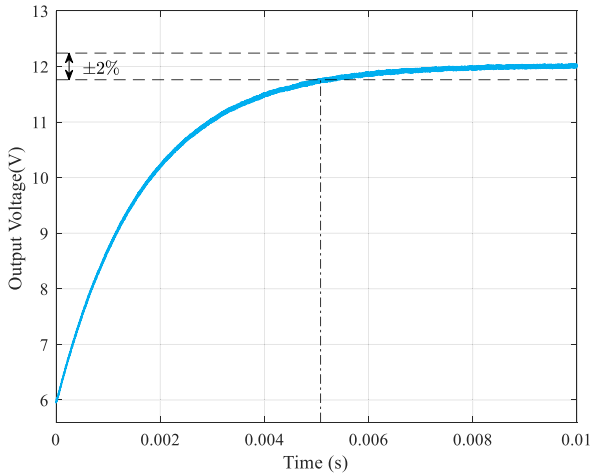

Fig. 16. Step response of output voltage with α of MFC-1.a for model variation space 1 in Table III.

VI. Experimental Results

Seven buck converter prototypes with different circuit parameters are built to evaluate the findings above (see Fig. 15). All controllers are designed as per Section V to give a $t_{set\_n} = 5$ ms and implemented by TMS320F28335 from Texas Instruments with a natural sampling frequency (sampling and processing the data once per switching cycle) of 100 kHz. The circuit and controller parameters used are identical to those in Section V. Controllers are discretized using the backward Euler method. Unless otherwise indicated, the nominal circuit and controller parameters based on MFC-1 are used.

The plotted data of Figs. 16–22 are first captured by Keysight MSOX3024A oscilloscope from the experiment in .cvs format and then plotted with the aid of MATLAB. In this way, the step responses of the closed-loop system in different scenarios can be plotted in one figure to facilitate the comparisons of the performance robustness.

A. Evaluation of the New Modeling Tools

Fig. 16 illustrates the step response of v_o when its reference v_o^* changes from 6 to 12 V. The v_o response measures a $t_{set} = 5.08$ ms, which aligns with the design and well matches that predicted by (10). In contrast, the existing interpretation

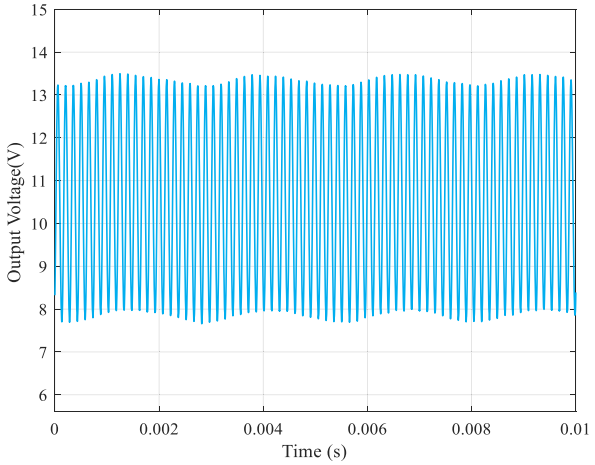

Fig. 17. Steady-state voltage waveforms after a reference step with 1/8 of α of MFC-1.a for model variation space 1 in Table III.

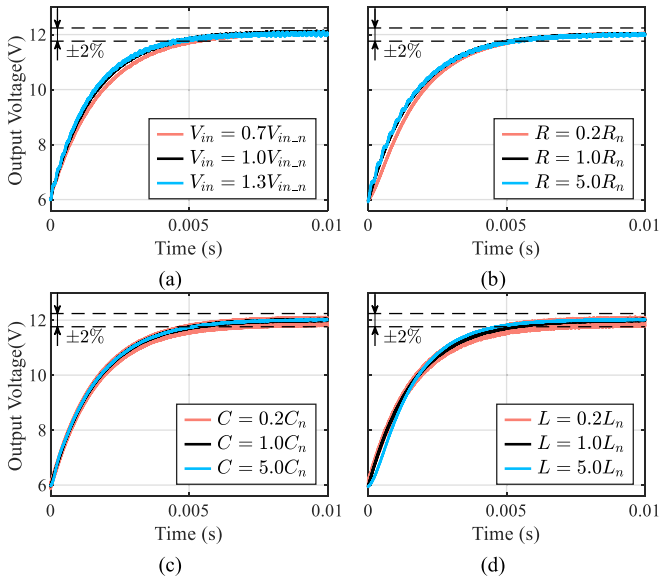

Fig. 18. Step response of output voltage with MFC-1.a against variations in (a) V_{in}, (b) R, (c) C, and (d) L.

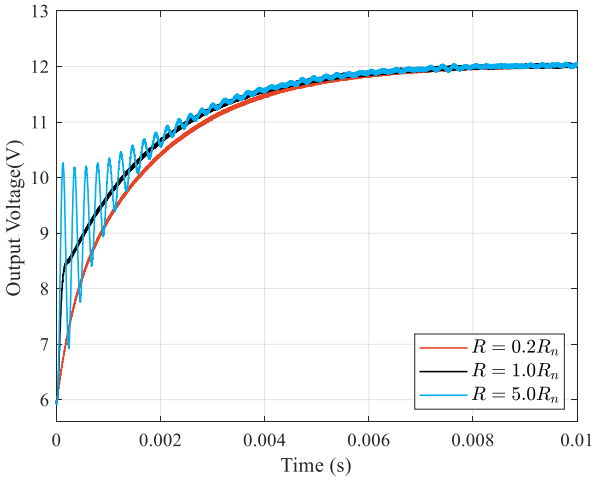

Fig. 19. Step response of output voltage against variation in R with i-P for model variation space 1 in Table III.

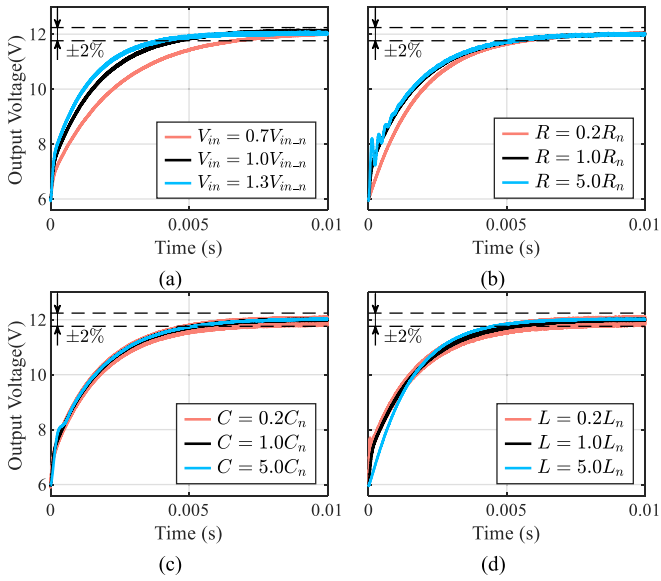

Fig. 20. Step response of output voltage with PI controller against variations in (a) V_{in} (b) R, (c) C, and (d) L.

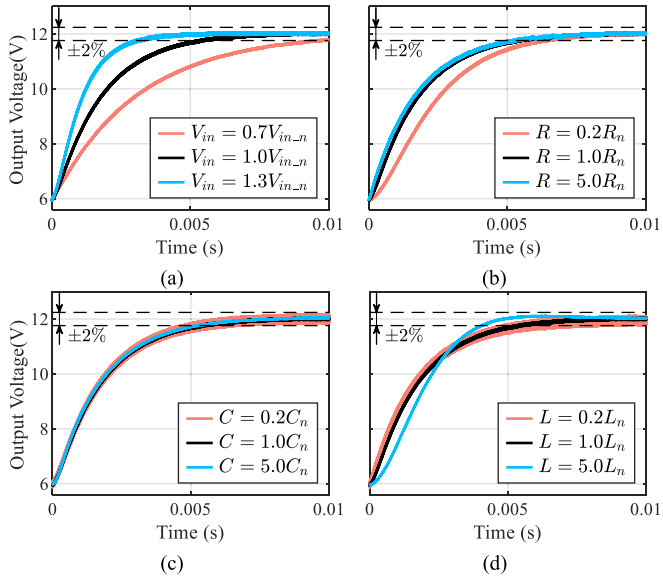

Fig. 21. Step response of output voltage with MFC-1.c against variations in (a) V_{in} (b) R, (c) C, and (d) L.

based on (7) predicts $t_{set} = 4/k = 2$ ms according to the first-order dynamic response formula, showing a 60% prediction error.

In Fig. 17, the same experiment is repeated, except that the inner loop term α is reduced to $\alpha/8$. Instability is observed, as precisely predicted by Fig. 6. The existing interpretations of MFC, however, predict that the system is invariably stable.

The above two experiments confirm the capabilities of the new modeling tools in the prediction of system dynamics and stability with MFC. The results also show that a MFC system does not yield a dynamic response and stability which is solely governed by the outer-loop controller k. The inner loop terms are also attributed.

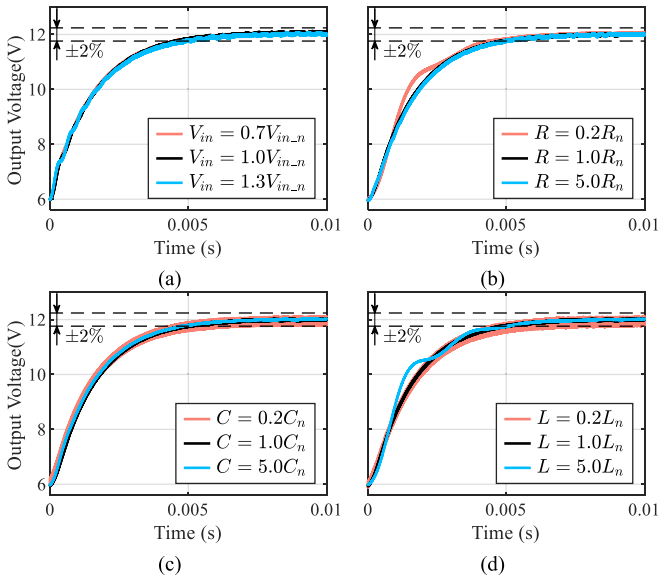

Fig. 22. Step response of output voltage with MFC-2 against variations in (a) V_{in}, (b) R, (c) C, and (d) L.

TABLE IV
DYNAMIC RESPONSE RESULTS WITHIN MODEL VARIATION SPACE 1

Control	MFC-1.a		MFC-1.c		PI		MFC-2	
	t_{set} (ms)	e_r (%)	t_{set} (ms)	e_r (%)	t_{set} (ms)	e_r (%)	t_{set} (ms)	e_r (%)
Nom	5.08	/	5.42	/	5.19	/	4.85	/
$0.2R_n$	5.37	5.7	6.25	15.3	5.66	9.1	4.74	2.3
$5R_n$	5.11	0.6	5.33	1.7	5.20	0.2	4.75	2.1
$0.2C_n$	5.18	2.0	5.36	1.1	5.26	1.3	4.83	0.4
$5C_n$	5.13	1.0	5.26	3.0	5.27	1.5	4.83	0.4
$0.2L_n$	5.18	2.0	5.27	2.8	5.10	1.7	4.96	2.3
$5L_n$	4.61	9.3	3.54	34.7	4.47	13.9	4.80	1.0

TABLE V
DYNAMIC RESPONSE RESULTS WITHIN MODEL VARIATION SPACE 2

Control	MFC-1.a		MFC-1.c		PI		MFC-2	
	t_{set} (ms)	e_r (%)	t_{set} (ms)	e_r (%)	t_{set} (ms)	e_r (%)	t_{set} (ms)	e_r (%)
Nom	4.88	/	5.42	/	5.15	/	4.90	/
$0.7V_{in\_n}$	5.53	13.3	9.57	76.6	7.11	38.1	4.85	1.0
$1.3V_{in\_n}$	4.67	4.3	3.00	44.6	4.06	21.2	4.96	1.2

B. Evaluation of Model Dependencies of MFC

To demonstrate the model dependence nature of MFC, we vary the circuit parameters (R, C, L) and operating point (V_{in}) with respect to their nominal values, each at a time, by fivefold and 30%, respectively, and repeat the same step response test.

Fig. 18 captures the measured v_o waveforms. From these measurements, excursions of t_{set} from $t_{set\_n} = 5$ ms can be visualized. Tables IV and V record the measured t_{set} and e_r for each case. These results show an $e_{r\cdot max} = 9.3\%$ regarding R, C, L variations, and 13.3% regarding V_{in} variations, confirming the model-dependent nature of a MFC system. The results also align with those shown in Figs. 13 and 14 at A2 and B2, further confirming the accuracies of the new modeling tools.

C. Evaluation of Stability of Conventional MFC

To verify that if $I(s) = L(s) = s$, the i-P type MFC tends to be unstable whereas $L(s) = 0$ can improve its stability, simulation results of output voltage step responses with R variation based on MFC-1 and i-P with LPF are compared.

Fig. 19 shows output voltage step responses of the conventional i-P controller against variation in R. These results show that the output voltage of i-P control presents high oscillation when $R = 5R_n$, tending to be unstable. Compared with that of MFC-1 ($L(s) = 0$) shown in Fig. 18(b), the results demonstrate that MFC-1 without feedforward can gain better stability considering model variation.

D. MFC-1 Versus Single-Loop Controller

The same experiments as those in Section VI-B are further repeated, but with the optimized PI and a nonoptimized MFC-1 controller (i.e., MFC-1.c in Section V-C), respectively. Fig. 20 captures the associated v_o waveforms with PI controller, and Tables IV and V show the detailed t_{set} and e_r. As shown, $e_{r\cdot max} = 13.9\%$ regarding R, C, L variations, and 38.1% regarding V_{in} variations. Compared to the results with MFC-1.a, the PI controller shows a greater e_r in all tested cases, and thus less performance robustness against model variations.

Fig. 21 shows v_o waveforms with the nonoptimized MFC-1 controller. The corresponding data are also recorded in Tables IV and V. As shown, $e_{r\cdot max} = 36.7\%$ regarding R, C, L variations, and 76.7% regarding V_{in} variations. Compared with the PI controller, it has greater e_r in all tested cases, confirming that MFC with $\|1+T\| < 1$ can lead to worse performance robustness than a single-loop controller.

E. Evaluation of MFC-2

Finally, the step-change experiments in Section VI-B are repeated with MFC-2. Fig. 22 illustrates v_o waveforms. Tables IV and V record the measured results. In particular, MFC-2 shows an $e_{r\cdot max} = 2.3\%$ regarding R, C, L variations, and 1.2% regarding V_{in} variations, which are almost negligible. The results match our prediction in Figs. 13 and 14, and support the opportunities of quasi-model-free operation and design.

Compared to PI and MFC-1.a controller, MFC-2 controller effectively reduces $e_{r\cdot max}$ by 83.5% and 75.3%, respectively, regarding R, C, L variations, and 96.8% and 91.0%, respectively, regarding V_{in} variations. These results well demonstrate the supremacy of performance robustness of the MFC-2 method.

It is also measured that the execution time of PI, MFC-1, and MFC-2 are 1.55 μs, 1.65 μs, and 1.94 μs, respectively. It shows that the execution time of both MFC-1 and MFC-2 is comparable to that of PI. This observation is consistent with our analysis shown in Section II-B, which MFC is dataset and computational light.

To further evaluate the performance robustness with respect to varying references, we perform similar tests as above for PI, MFC-1, and MFC-2 controllers in the case of a varying reference (same as that in [51], particularly, with an initial reference voltage at 12 V and ending at 11 V). These tests

TABLE VI
ITAE COMPARISON WITHIN MODEL VARIATION SPACE 2

Control	MFC-1.a	PI	MFC-2
ITAE with V_{in_n} (V·s)	1.9765	1.7163	2.1259
ITAE with $0.7V_{in\_n}$ (V·s)	2.4728	2.4139	2.1278
ITAE with $1.3V_{in\_n}$ (V·s)	1.6952	1.3178	2.1243
Max relative ITAE error (%)	39.34	76.78	0.16

are conducted in PSIM simulation due to hardware limitation. All controllers under test have identical parameters to the experiments, as shown in model variation space 2 in Table III. The output voltage data are collected and integral time absolute errors (ITAE) regarding the output voltage tracking error of three controllers are compared in Table VI. The maximum relative errors with respect to ITAE under nominal input V_{in_n} are used as a benchmark for comparing the performance robustness of the different controllers. The results also show that MFC-1 can achieve better performance robustness than PI, and MFC-2 has the most robust performance, which is consistent with the conclusions drawn above.

VII. CONCLUSION

This article critically examines Fliess's MFC technique, using the classical control theory as a basic tool. The basic principle of MFC is highlighted. It is shown that MFC is essentially a special form of cascaded control with one feedback signal, and thus MFC in principle is model-dependent instead of being model-free. However, it is also found that MFC can be designed more performance robust than single-loop linear controllers if the magnitude of MFC's inner loop gain is designed much greater than unity below the bandwidth frequency. On top of that, it is also shown that stability margin imposes a major hindrance to elevating the inner loop gain and thus the performance robustness. To solve this issue, a new MFC, MFC-2, is proposed with the aid of the generalized MFC framework. Case studies and associated experiments on a buck converter example, of which the switching cycle averaged plant model is a single-input-single-output linear system, are conducted to verify the new understanding and conclusions drawn above.

For future work, we aim to apply the revisited theory of MFC to more complicated application scenarios, including MIMO systems (e.g., electrical machine drive systems) and nonlinear systems (e.g., dynamic wireless charging systems), and extend our linear analyzing framework to nonlinear MFC such as model-free predictive control, and compare the method with prevalent control methods. Besides, based on some recent studies, such as variable-α method [6], marine predators algorithm [47], and extremum-seeking control [48], the design of MFC can be further studied to help achieve model-free design. Furthermore, the stability margin of MFC will be further investigated.

REFERENCES

[1] R. C. Dorf and R. H. Bishop, *Modern Control Systems*, 12th ed. Englewood Cliffs, NJ, USA: Prentice-Hall, 2011.

[2] S. Kapat and P. T. Krein, "A tutorial and review discussion of modulation, control and tuning of high-performance DC-DC converters based on small-signal and large-signal approaches," *IEEE Open J. Power Electron.*, vol. 1, pp. 339–371, 2020.

[3] K. J. Åström and R. M. Murray, *Feedback Systems: An Introduction for Scientists and Engineers*, vol. 46. Princeton, NJ, USA: Princeton Univ. Press, 2008.

[4] O. A. Somefun, K. Akingbade, and F. Dahunsi, "The dilemma of PID tuning," *Annu. Rev. Control*, vol. 52, pp. 65–74, Jun. 2021.

[5] K. J. Åström and T. Hägglund, *Advanced PID Control*. Durham, NC, USA: Instrum. Soc. Amer., 2006.

[6] I. Landau, R. Lozano, M. M'Saad, and A. Karimi, *Adaptive Control: Algorithms, Analysis and Applications*. 2nd ed. Berlin, Germany: Springer, 2011.

[7] S. C. Tan, Y. M. Lai, and C. K. Tse, "General design issues of sliding-mode controllers in DC-DC converters," *IEEE Trans. Ind. Electron.*, vol. 55, no. 3, pp. 1160–1174, Mar. 2008.

[8] J. Rodriguez, P. Cortes, R. Kennel, and M. P. Kazmierkowski, "Model predictive control—A simple and powerful method to control power converters," *IEEE Trans. Ind. Electron.*, vol. 56, no. 6, pp. 1826–1838, Jun. 2009.

[9] A. O'Dwyer, *Handbook of PI and PID Controller Tuning Rules*. 3rd ed., London, U.K.: Imperial College Press, 2009.

[10] J. Koelsch, "Tuning tools maintain harmony in PID loops," 2014. Accessed: Feb. 21, 2014. [Online]. Available: https://www.automationworld.com/products/software/article/13311005

[11] R. Ionutiu et al., "Real-time simulation for power electronics in railway applications and beyond," *ABB Rev.*, vol. 34, pp. 34–39, 2014.

[12] L. Beaudouin, R. Chen, R. Fletcher, and S. V. Popup, "The need for speed: Accelerating product improvement at industrials," *McKinsey Highlights*, pp. 1–13, May 2020.

[13] K. Hermanns, Y. Peng, and A. Mantooth, "The increasing role of design automation in power electronics: Gathering what is needed," *IEEE Power Electron. Mag.*, vol. 7, no. 1, pp. 46–50, Mar. 2020.

[14] B. Park and M. M. Olama, "A model-free voltage control approach to mitigate motor stalling and FIDVR for smart grids," *IEEE Trans. Smart Grid*, vol. 12, no. 1, pp. 67–78, Jan. 2021.

[15] K. Zhao et al., "Robust model-free nonsingular terminal sliding mode control for PMSM demagnetization fault," *IEEE Access*, vol. 7, pp. 15737–15748, 2019.

[16] J. Villagra and C. Balaguer, "Robust motion control for humanoid robot flexible joints," in *Proc. 18th Mediterranean Conf. Control Automat.*, Marrakech, Morocco, 2010, pp. 963–968.

[17] L. Menhour, B. D'Andrea-Novel, M. Fliess, D. Gruyer, and H. Mounier, "An efficient model-free setting for longitudinal and lateral vehicle control: Validation through the interconnected Pro-sivic/RTmaps prototyping platform," *IEEE Trans. Intell. Transp. Syst.*, vol. 19, no. 2, pp. 461–475, Feb. 2018.

[18] L. Michel, C. Join, M. Fliess, P. Sicard, and A. Cheriti, "Model-free control of dc /dc converters," in *Proc. IEEE 12th Workshop Control Model. Power Electron*, Boulder, CO, USA, 2010, pp. 1–8.

[19] L. Cao, H. Li, and H. Zhang, "Model-free power control of front-end PFC AC/DC converter for on-board charger," in *Proc. IEEE 8th Int. Power Electron. Motion Control Conf.*, 2016, pp. 2719–2723.

[20] A. Barkat, B. Marinescu, C. Join, and M. Fliess, "Model-free control for VSC-based HVDC systems," in *Proc. IEEE PES Innov. Smart Grid Technol. Conf. Eur.*, Sarajevo, Bosnia and Herzegovina, 2018, pp. 1–6.

[21] Y. Hong, D. Xu, W. Yang, B. Jiang, and X. G. Yan, "A novel multi-agent model-free control for state-of-charge balancing between distributed battery energy storage systems," *IEEE Trans. Emerg. Topics Comput. Intell.*, vol. 5, no. 4, pp. 679–688, Aug. 2021.

[22] A. Boubakir, S. A. Touil, S. Labiod, and N. Boudjerda, "A robust model-free controller for a three-phase grid-connected photovoltaic system based on ultra-local model," *Protection Control Modern Power Syst.*, vol. 6, no. 1, 2021, Art. no. 43.

[23] X. Liu, Y. Zhang, H. Yang, and J. Rodriguez, "Model-Free predictive current control for three-phase power converters with LCL filter," in *Proc. IEEE Energy Convers. Congr. Expo.*, 2020, no. 1, pp. 5916–5921.

[24] Y. Zhang, L. Bingyu, J. Liu, and X. Liu, "Model-Free predictive current control of PWM rectifier under unbalanced and distorted network," in *Proc. IEEE Energy Convers. Congr. Expo.*, 2020, pp. 5944–5951.

[25] H. Sira-Ramirez, "Vers une commande multivariable sans mod'ele," in *Proc. Conf. Int. Francophone D'automatique*, Bordeaux, France, 2006, pp. 1–8.

[26] M. Fliess, C. Join, and H. Sira-Ramírez, "Complex continuous nonlinear systems: Their black box edentification and their control," *IFAC Proc. Vol.*, vol. 39, no. 1, pp. 416–421, 2006.
[27] J. Duan et al., "Deep-reinforcement-learning-based autonomous voltage control for power grid operations," *IEEE Trans. Power Syst.*, vol. 35, no. 1, pp. 814–817, Jan. 2020.
[28] Z. Hou and S. Jin, *Model Free Adaptive Control: Theory and Applications*. Raton Boca, FL, USA: CRC Press, 2013.
[29] M. Fliess and C. Join, "Model-free control," *Int. J. Control*, vol. 86, no. 12, pp. 2228–2252, 2013.
[30] L. Menhour, B. D'Andrea-Novel, M. Fliess, and H. Mounier, "Multivariable decoupled longitudinal and lateral vehicle control: A model-free design," in *Proc. 52nd IEEE Conf. Decis. Control*, Firenze, Italy, 2013, pp. 2834–2839.
[31] Y. Al Younes, A. Drak, H. Noura, A. Rabhi, and A. El Hajjaji, "Model-free control of a quadrotor vehicle," in *Proc. Int. Conf. Unmanned Aircr. Syst.*, Orlando, FL, USA, 2014, pp. 1126–1131.
[32] S. Zhao, F. Blaabjerg, and H. Wang, "An overview of artificial intelligence applications for power electronics," *IEEE Trans. Power Electron.*, vol. 36, no. 4, pp. 4633–4658, Apr. 2021.
[33] O. Bara, M. Fliess, C. Join, J. Day, and S. M. Djouadi, "Toward a model-free feedback control synthesis for treating acute inflammation," *J. Theor. Biol.*, vol. 448, pp. 26–37, 2018.
[34] H. Yuan, S. Li, S. C. Tan, and R. S. Y. Hui, "Simplified algebraic estimation technique for sensor count reduction in single-phase converters with an active power buffer," *IEEE Trans. Power Electron.*, vol. 36, no. 10, pp. 11444–11455, Oct. 2021.
[35] M. H. Khooban, M. Gheisarnejad, H. Farsizadeh, A. Masoudian, and J. Boudjadar, "A new intelligent hybrid control approach for DC-DC converters in zero-emission ferry ships," *IEEE Trans. Power Electron.*, vol. 35, no. 6, pp. 5832–5841, Jun. 2020.
[36] Y. Zhang, J. Jin, and L. Huang, "Model-free predictive current control of PMSM drives based on extended state observer using ultralocal model," *IEEE Trans. Ind. Electron.*, vol. 68, no. 2, pp. 993–1003, Feb. 2021.
[37] S. Abrazeh, A. Parvaresh, S. R. Mohseni, M. J. Zeitouni, M. Gheisarnejad, and M. H. Khooban, "Nonsingular terminal sliding mode control with ultra-local model and single input interval Type-2 fuzzy logic control for pitch control of wind turbines," *IEEE/CAA J. Automatica Sinica*, vol. 8, no. 3, pp. 690–700, Mar. 2021.
[38] X. Zhang, H. Wang, Y. Tian, L. Peyrodie, and X. Wang, "Model-free based neural network control with time-delay estimation for lower extremity exoskeleton," *Neurocomputing*, vol. 272, pp. 178–188, 2018.
[39] M. Fliess and C. Join, "Stability margins and model-free control: A first look," in *Proc. Eur. Control Conf.*, Strasbourg, France, 2014, pp. 454–459.
[40] F. Golnaraghi and B. C. Kuo, *Automatic Control Systems*, 9th ed. London, U.K.: Prentice Hall International, 2017.
[41] P. A. Gédouin, E. Delaleau, J. M. Bourgeot, C. Join, S. A. Chirani, and S. Calloch, "Experimental comparison of classical PID and model-free control: Position control of a shape memory alloy active spring," *Control Eng. Pract.*, vol. 19, no. 5, pp. 433–441, 2011.
[42] V. Milanés, J. Villagrá, J. Godoy, and C. González, "Comparing fuzzy and intelligent PI controllers in stop-and-go manoeuvres," *IEEE Trans. Control Syst. Technol.*, vol. 20, no. 3, pp. 770–778, May 2012.
[43] T. MohammadRidha et al., "Model free iPID control for glycemia regulation of type-1 diabetes," *IEEE Trans. Biomed. Eng.*, vol. 65, no. 1, pp. 199–206, Jan. 2018.
[44] M. Fliess and C. Join, "Intelligent PID controllers," in *Proc. 16th Mediterranean Conf. Control Automat.*, Ajaccio, France, 2008, pp. 326–331.
[45] R. E. Precup, M. B. Radac, R. C. Roman, and E. M. Petriu, "Model-free sliding mode control of nonlinear systems: Algorithms and experiments," *Inf. Sci. (New York)*, vol. 381, pp. 176–192, 2017.
[46] X. Dong, H. Li, H. Zhang, J. Gu, C. Pan, and L. Liu, "Model-free predictive control for power decoupling integrated PFC converters," in *Proc. 22nd Int. Conf. Elect. Mach. Syst.*, Harbin, China, 2019, pp. 1–5.
[47] Q. Wu, H. Wang, and Y. Tian, "Model free control based nonlinear integral-backstepping control for blood glucose regulation," in *Proc. IEEE 6th Data Driven Control Learn. Syst. Conf.*, Chongqing, China, 2017, pp. 94–99.
[48] B. D'Andréa-Novel, M. Fliess, C. Join, H. Mounier, and B. Steux, "A mathematical explanation via 'intelligent' PID controllers of the strange ubiquity of PIDs," in *Proc. 18th Mediterranean Conf. Control Automat.*, 2010, no. 5, pp. 395–400.
[49] B. Carter and R. Mancini, *OP AMPS For Everyone*, 5th ed., Amsterdam, Netherlands: Elsevier, 2018.
[50] D. O. Boillat, F. Krismer, and J. W. Kolar, "Design space analysis and ρ-η pareto optimization of LC output filters for switch-mode AC power sources," *IEEE Trans. Power Electron.*, vol. 30, no. 12, pp. 6906–6923, Dec. 2015.
[51] B. Park, Y. Zhang, M. Olama, and T. Kuruganti, "Model-free control for frequency response support in microgrids utilizing wind turbines," *Elect. Power Syst. Res.*, vol. 194, May 2021, Art. no. 107080.

Wanrong Li received the B.E. degree in electrical engineering and automation from North China Electric Power University, Beijing, China, in 2016, and the M.E. degree in electrical engineering from Xi'an Jiaotong University, Xi'an, China, in 2019. She is currently working toward the Ph.D. degree in controller design automation techniques with the School of Electrical and Information Engineering, the University of Sydney, Australia.

Her current research interests include design and optimization of modern control techniques, and applications in power electronic systems.

Huawei Yuan (Member, IEEE) received the B.Eng. and M.S. degrees in electrical engineering from Tsinghua University, Beijing, China, in 2013 and 2016, respectively, and the Ph.D. degree in electrical and electronic engineering from The University of Hong Kong, Hong Kong, in 2020.

He is currently a Research Fellow with the School of Electrical and Electronic Engineering, Nanyang Technological University. His current research interests focus on the control of power electronic systems and the smart grid.

Sinan Li (Member, IEEE) received the B.S. degree in electrical engineering from the Harbin Institute of Technology, Harbin, China, in 2009 and the Ph.D. degree in electrical and electronic engineering from The University of Hong Kong, Hong Kong, in 2014.

He has been with The University of Bath, U.K., and The University of Hong Kong, Hong Kong, as an Assistant Professor and Postdoctoral Research Fellow, respectively. He is currently an Assistant Professor with the School of Electrical and Information Engineering, The University of Sydney, Australia. He has authored or coauthored more than 50 transaction and conference papers and holds five worldwide patents (three transferred to industry). His research interest includes all areas of power electronics.

Dr. Li is the Discovery Early Career Research Award (DECRA) Fellow of Australian Research Council. He was a Founding Member of the IEEE-Eta Kappa Nu (HKN) at The University of Hong Kong. He was a recipient of the Best Paper Award (Second Place) of the IEEE TRANSACTIONS ON POWER ELECTRONICS in 2019. He serves as a Guest Associate Editor for IEEE JOURNAL OF EMERGING AND SELECTED TOPICS OF CIRCUITS AND SYSTEMS.

Jianguo Zhu (Senior Member, IEEE) received the B.E. degree from Jiangsu Institute of Technology, China, in 1982, the M.E. degree from Shanghai University of Technology, China, in 1987, and the Ph.D. degree in 1995 from the University of Technology Sydney (UTS), Australia, all in electrical engineering.

He was appointed a Lecturer at UTS in 1994 and promoted to a Full Professor in 2004 and a Distinguished Professor of electrical engineering in 2017. At UTS, he has held various leadership positions, including the Head of School for School of Electrical, Mechanical and Mechatronic Systems and the Director for Centre of Electrical Machines and Power Electronics. In 2018, he joined the University of Sydney, Australia, as a Full Professor and the Head of the School for School of Electrical and Information Engineering. His research interests include computational electromagnetics, measurement and modelling of magnetic properties of materials, electrical machines and drives, power electronics, renewable energy, microgrids, and digital energy systems.